crystals

Brief Report

Interfacial Characterization of Selective Laser Melting of a SS316L/NiTi Multi-Material with a High-Entropy Alloy Interlayer

Arseniy Repnin *, Artem Kim and Anatoliy Popovich

Institute of Machinery, Materials, and Transport, Peter the Great St. Petersburg Polytechnic University (SPbPU), Polytechnicheskaya, 29, 195251 Saint Petersburg, Russia
* Correspondence: repnin_arseniy@mail.ru

Abstract: Some multi-materials produced via SLM and containing 316L steel may exhibit defects and cracks in the interfacial zone. There is a lack of research on 316L/NiTi multi-materials with an interlayer produced via SLM. This study aims to investigate the influence of a high-entropy alloy (HEA)—CoCrFeNiMn interlayer on the defects' formation, microstructure, phase, and chemical compositions, as well as the hardness of the interfacial zone. It was concluded that using of high-entropy alloy as an interlayer in the production of 316L/HEA/NiTi multi-material via SLM is questionable, since numerous cracks and limited pores occurred in the HEA/NiTi interfacial zone. The interfacial zone has an average size of 100–200 µm. Microstructure studies indicate that island macrosegregation is formed in the interfacial zone. The analysis of phase, chemical composition, and hardness demonstrates that a small amount of FeTi may form in the island macrosegregation. The increase in iron content in this area could be the reason for this. The interfacial zone has a microhardness of about 430 HV, and in the island macrosegregation, the microhardness increases to about 550 HV. Further research could involve an in-depth analysis of the phase and chemical composition, as well as examining other metals and alloys as interlayers.

Keywords: additive manufacturing; selective laser melting; multi-material; SS316L/NiTi; HEA interlayer; interfacial zone

check for updates

Citation: Repnin, A.; Kim, A.; Popovich, A. Interfacial Characterization of Selective Laser Melting of a SS316L/NiTi Multi-Material with a High-Entropy Alloy Interlayer. *Crystals* **2023**, *13*, 1486. https://doi.org/10.3390/cryst13101486

Academic Editor: Sanbao Lin

Received: 30 August 2023
Revised: 28 September 2023
Accepted: 4 October 2023
Published: 12 October 2023

1. Introduction

Recently, there has been a significant increase in the use of additive manufacturing (AM) in high-tech industries such as petrochemical, mechanical engineering, electrical power, biomedicine, etc. [1,2]. This is mainly due to the ability of this technology to produce complex products at lower costs in comparison to traditional methods [3]. One type of AM, known as selective laser melting (SLM), can be utilized to produce metal products [4–6], as well as multi-materials with variable chemical compositions [7,8]. The implementation of this approach enhances the performance characteristics of these products [9].

In recent years, there has been significant research on multi-materials containing stainless steel obtained via SLM [10–12], and several studies have examined defects in the interfacial zone in these multi-materials. In the interfacial zone of 316L/CuSn10 multi-materials, dendritic cracks propagate orthogonally to the 316L region from the melting zone [13,14]. Defects and cracks are observed in the interfacial zone of 316L/IN718 multi-materials and carbides such as NbC and TiC [15,16]. Cracks occur in the interfacial zone of 316L/$Ni_{50.83}Ti_{49.17}$ multi-material, possibly caused by the presence of brittle intermetallic compounds (Fe_2Ti, $FeNi_3$, Ti_2Ni) [17].

It should be noted that the 316L/NiTi multi-material obtained via SLM is of great interest [18]. However, this multi-material, like the other multi-materials with 316L mentioned above, may exhibit defects and cracks in the interfacial zone. The cause of these cracks may be attributed to phase formation. Traditional technologies employ interlayers to reduce such effects in multi-materials production. In the 316L/NiTi multi-materials, interlayers such as Ta, Ni, FeNi alloy, and high-entropy alloy (HEA) reduce the amount of brittle intermetallic compounds (IMCs) [19–22].

During the laser welding of NiTi to 316L, a non-uniform chemical composition distribution occurs, and the crystallization mode changes from planar to dendritic form. The addition of the Ta interlayer results in an increase in the formation of $TaCr_2$ and Ni_3Ta and a decrease in the brittle IMCs ($TiFe_2$, $TiCr_2$, TiFe, etc.) in the weld joint [19]. A similar situation occurs when a Ni interlayer is used, leading to the formation of mainly Ni-rich IMCs (Fe_3Ni and Ni_3Ti) instead of brittle IMCs (Fe_2Ti, Cr_2Ti, and Ti_2Ni) [20]. During electron beam welding, when Ni and FeNi interlayers are used, the microstructure of the weld zone has two different regions that consist of austenite and the IMCs (Fe_2Ti, Ni_3Ti). The volume fraction of the IMC regions is different [21]. During laser welding, when an HEA (CoCrFeNiMn) interlayer is added, island macrosegregations are formed by the Marangoni effect. After the addition of the HEA interlayer, its elements get into the weld, which reduces the formation of brittle IMCs [22].

Currently, there is a lack of research on 316L/NiTi multi-materials with an interlayer produced via SLM. Consequently, this study is aimed at investigating the influence of an HEA—CoCrFeNiMn interlayer on the defects' formation, microstructure, phase, and chemical composition, as well as the hardness of the interfacial zone between the HEA and NiTi.

2. Materials and Methods

2.1. Starting Materials

Metallic spherical powders of 316L, HEA CoCrFeNiMn, and NiTi alloys were utilized to obtain the multi-material 316L/HEA/NiTi samples via SLM (Table 1 and Figure 1). The 316L (SferaM LLC, Metlino, Russia) and NiTi (TLS Technik GmbH&Co., Bitterfeld, Germany) metallic powders were manufactured through atomization. To obtain HEA powder, mechanical alloying was carried out via a Fritsch Pulverisette 4 planetary mill (Fritsch GmbH, Idar-Oberstein, Germany). Following mechanical alloying, the particles were spheroidized employing a Tekna TEK-15 system (Tekna, Sherbrooke, QC, Canada). The particle size distribution of the powders was measured using a laser diffraction particle size analyzer, Analysette 22 NanoTec Plus (Fritsch GmbH, Idar-Oberstein, Germany, Table 2).

Table 1. Chemical composition of 316L, HEA, and NiTi metallic powders.

Alloy	Fe, %	Cr, %	Ni, %	Co, %	Mn, %	Mo, %	Ti, %
316L	base	16.5–18.5	10–13	-	2 (max)	2–2.5	-
HEA	20	20	20	20	20	-	-
NiTi	-	-	50	-	-	-	50

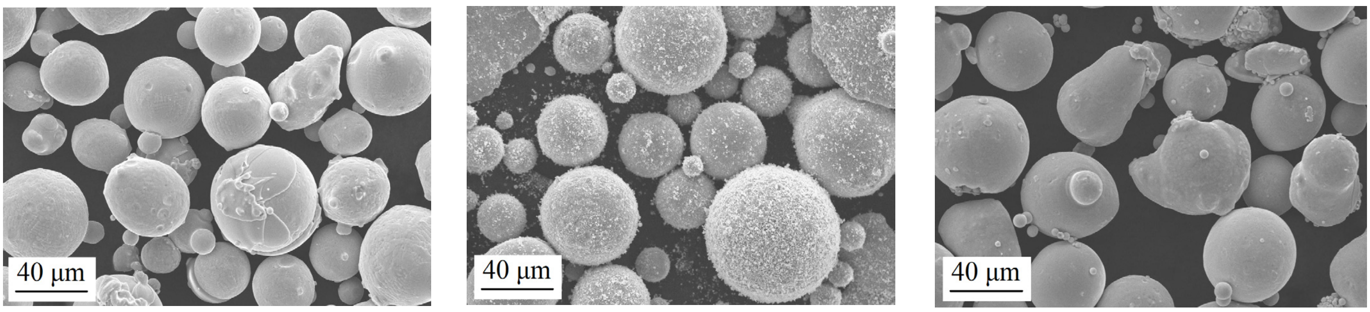

(**a**) (**b**) (**c**)

Figure 1. Morphology of metallic powders: (**a**) 316L, (**b**) HEA, and (**c**) NiTi.

Table 2. The particle size distribution of 316L, HEA, and NiTi metallic powders.

%	316L	HEA	NiTi
	<µm	<µm	<µm
10	20	18	21
50	39	53	38
90	70	103	67

2.2. The SLM Process Parameters

During the fabrication of the multi-material 316L/HEA/NiTi samples via SLM, the HEA alloy was built onto the 316L alloy, followed by the NiTi alloy onto the HEA. HEA samples were successfully obtained via SLM, and the energy density for this alloy was selected on the basis of this study [23]. For 316L and HEA alloys, the SLM parameters were chosen based on energy density according to existing data [24,25]. The SLM 280HL machine (SLM Solutions, Germany) was used for the manufacturing of the samples (Table 3).

Table 3. Process parameters of SLM for the multi-material 316L/HEA/NiTi samples.

Alloy	Scanning Speed, mm/s	Laser Power, W	Hatch Distance, µm	Layer Thickness, µm	Energy Density, J/mm^3
316L	760	275	100	50	72.37
HEA	650	360	120	50	92.31
NiTi	750	200	100	30	88.89

2.3. Characterizations

The microstructure was studied using a Leica DMi8 M optical microscope (Leica Microsystems, Wetzlar, Germany). Etching of the materials was performed utilizing Kroll's reagent comprising 83% distilled water, 14% HNO3, and 3% HF. In this study, a multi-material sample was analyzed. As different areas of the specimen necessitate varying etchants, a universal etchant does not exist for all three alloys. The focus was placed on the NiTi zone and Kroll's etchant. The chemical composition was analyzed using a Mira 3 scanning electron microscope (TESCAN, Brno, Czech Republic) with an energy-dispersive X-ray spectroscopy module. The phase composition was evaluated by X-ray microdiffraction with a beam width of 100 µm on a Rigaku SmartLab diffractometer (CuKα radiation, Rigaku Corporation, Tokyo, Japan). Microhardness was measured using a Vickers MicroMet 5101 microhardness tester (Buehler Ltd., Lake Bluff, IL, USA).

3. Results and Discussion

3.1. The Defect Analysis in the HEA/NiTi Interfacial Zone

The results of the defect analysis in the different zones are presented in Figure 2. The pure alloy zones exhibit no cracks and a few spherical pores. The minimal number of defects indicates that suitable printing parameters have been selected for pure alloys. The HEA/NiTi interfacial zone displays cracks and a pore. Presumably, the cracking may be attributed to the influence of the phase formation in the interfacial zone. As noted in the literature review, phase formation in the interfacial zone can lead to the formation of IMCs, which can be the cause of cracking. It has also been found that the using of an interfacial layer only reduces the amount of IMCs, but does not remove them completely. It can therefore be assumed that even with the presence of the HEA interlayer, brittle IMCs can occur in the multi-material. The interfacial zone exhibits significant mixing of the HEA and NiTi alloys and has an average size of 100–200 µm.

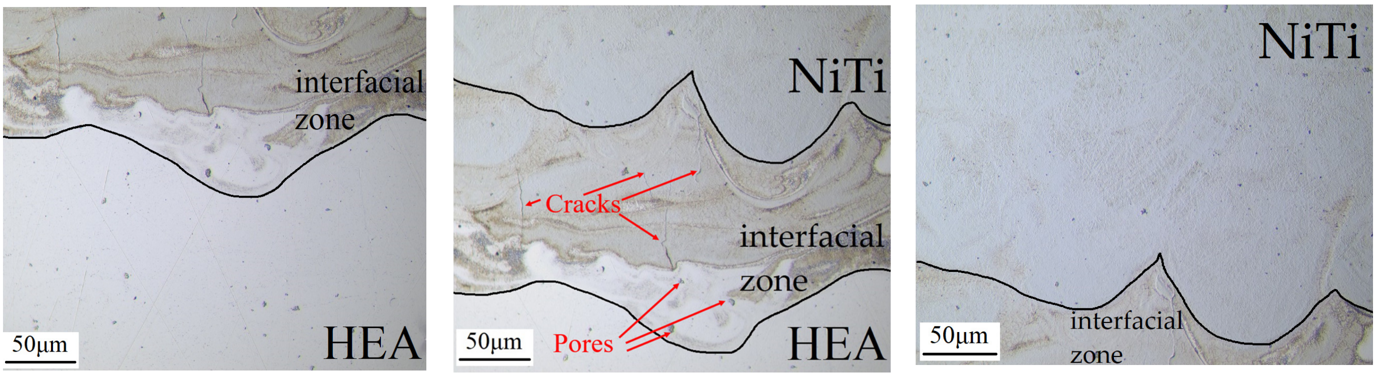

(**a**) (**b**) (**c**)

Figure 2. The results of the defect analysis in the different zones: (**a**) HEA, (**b**) HEA/NiTi interfacial zone, (**c**) NiTi.

3.2. The Phase Composition Analysis of the Multi-Material 316L/HEA/NiTi Sample

The results of the phase composition analysis are shown in Figure 3. In the pure alloy zones, the phase composition is consistent with these alloys: austenite (gamma-phase) in the 316L zone, a solid solution with an FCC structure in the HEA zone, and a B2 austenitic phase in the NiTi zone. The HEA/NiTi interfacial zone contains the B2 austenitic phase, along with a small amount of the intermetallic compound FeTi and solid solutions (Fe, Ni). It is hypothesized that the presence of a small amount of FeTi in the interfacial zone leads to the development of cracks, as this IMC causes embrittlement. It should be noted that the phase analysis of the interfacial zone was conducted using microanalysis mode, which could affect the accuracy of the results. Due to the small size of the analyzed area, the phase diagrams may not display all the phases. For instance, as stated in the following section, the presence of FeCr is assumed based on the chemical composition analysis, but it is not observed on the phase diagram.

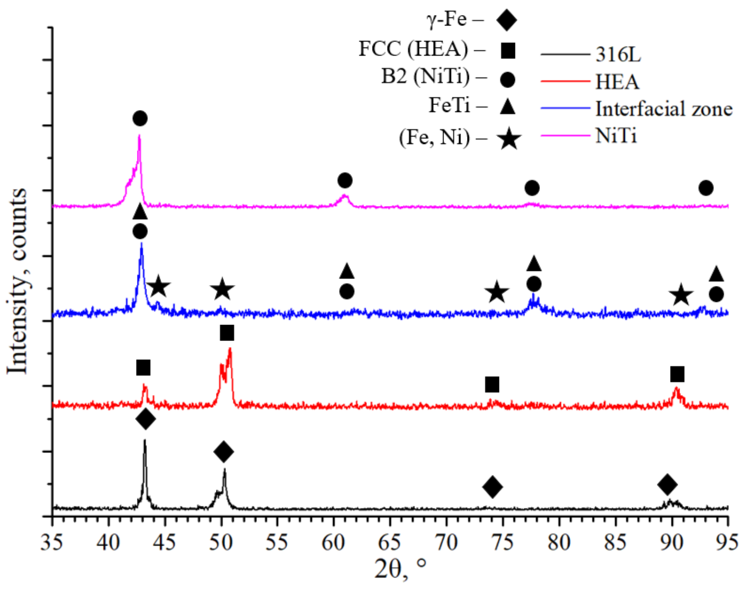

Figure 3. The phase composition of the multi-material 316L/HEA/NiTi sample.

3.3. The Microstructural and Chemical Composition Investigations, along with Hardness Analysis of the HEA/NiTi Interfacial Zone

The results of the microstructural and chemical composition investigations, along with the hardness analysis of the HEA/NiTi interfacial zone, are presented in Figure 4 and Table 4. The microstructural investigations reveal the development of island macrosegregation in the interfacial zone, which is attributed to the Marangoni effect [26]. The Marangoni effect occurs when the elevated temperature in the central region of the melt pool induces a reduction in surface tension, resulting in the molten metal flowing backward. A consistent energy input amplifies the backflow, leading it to return to the center of the melt pool, forming eddy currents [27]. Due to the rapid cooling and insufficient time for distributing the chemical elements of the HEA interlayer, inhomogeneities occur, leading to the formation of island macrosegregation in the eddy currents [22]. The microstructure in such regions consists of randomly distributed crystals around the eddy currents, which can be clearly seen in Figures 2b and 4b.

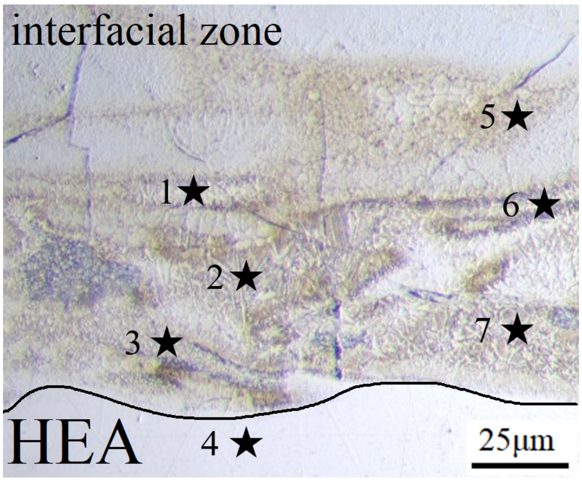

(a)

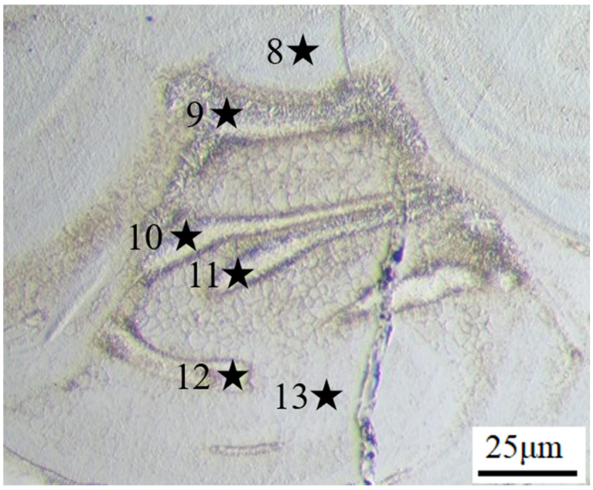

(b)

Figure 4. (**a**,**b**) Microstructure of the HEA/NiTi interfacial zone and EDS/hardness locations (black stars with numbers).

Table 4. Chemical composition of 316L, HEA, and NiTi metallic powders.

Position (from Figure 4)	Ni, at. %	Ti, at. %	Fe, at. %	Cr, at. %	Co, at. %	Mn, at. %	Hardness, HV	Potential Phases
1	32.7	27.18	15.44	12.19	8.34	3.89	546.9	FeTi, B2, (Fe, Ni), FeCr
2	33.53	25.96	14.72	12.15	9.2	4.06	564.4	
3	28.19	18.56	20.3	16.49	11.06	5.06	542.4	
4	19.93	1.16	31.40	23.62	16.37	7.12	191.2	(Fe, Ni), FeCr
5	36.96	33.66	11.48	9.08	6.44	2.39	432.7	B2, FeCr
6	33.48	29.4	13.89	11.43	8.07	3.47	564.8	FeTi, B2, (Fe, Ni), FeCr
7	33.11	24.26	15.51	12.89	9.74	4.22	557.6	
8	44.21	44.49	4.65	3.37	4.25	1.03	422.7	B2, FeCr
9	33.62	28.76	14.71	11.18	7.98	3.41	569.4	FeTi, B2, (Fe, Ni), FeCr
10	30.88	25.14	16.84	13.56	9.08	4.26	546.1	
11	29.16	25.27	18.26	14.06	8.65	4.33	558.9	
12	33.66	26.88	15.5	11.64	8.19	3.78	559.1	
13	38.57	34.77	10.31	7.87	5.87	2.39	445.9	B2, FeCr

From the chemical composition and hardness analyses, it becomes apparent that the interfacial zone consists predominantly of a B2 phase and that an additional phase is present, as the interfacial zone is harder than pure NiTi. Chemical composition analysis suggests that this phase may be FeCr. The microhardness of the interfacial zone is around 430 HV (points 5, 8, and 13). It can be assumed that in the island macrosegregations, the FeTi is formed, resulting in an increase in microhardness up to approximately 550 HV (points 1–3, 6–7, and 9–12). Point 4 lies outside the interfacial zone in the HEA zone comprising Fe, Ni, and FeCr, with a microhardness of approximately 190 HV (comparable to existing data [28]). The microhardness of pure NiTi was approximately 220 HV (comparable to existing data [29]). The hardness increases in the interfacial zone may indicate that new phases occur, which are different from those in the pure alloys. A comparable occurrence is visible in the interfacial zone during the welding of the NiTi with the stainless steel via laser welding [30]. The hardness increases in the island macrosegregations could indicate the presence of IMCs. The increase in iron content within the island macrosegregations, potentially leading to the formation of FeTi, is visible on the element distribution maps of the HEA/NiTi interfacial zone (Figure 5).

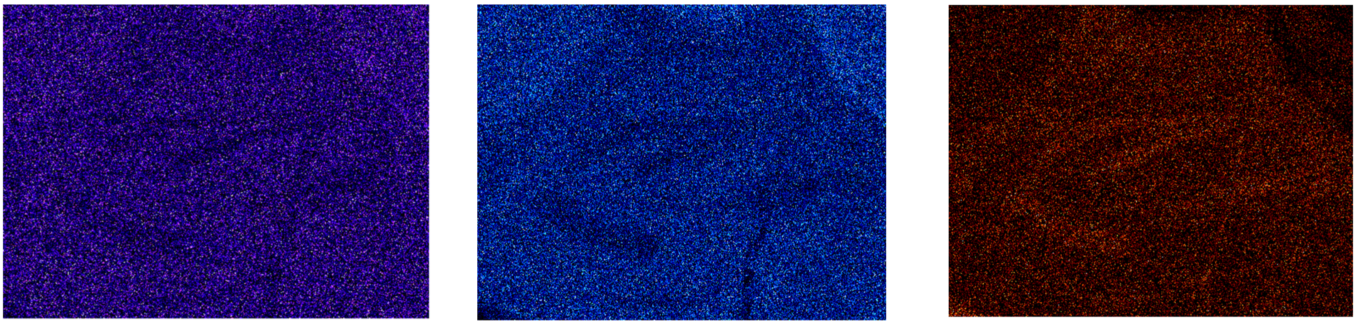

(**a**) (**b**) (**c**)

Figure 5. Elemental map of the HEA/NiTi interfacial zone (from Figure 4b): (**a**) Ni, (**b**) Ti, and (**c**) Fe.

4. Conclusions

Some multi-materials, produced via SLM and containing 316L steel, may exhibit defects and cracks in the interfacial zone. There is a lack of research on 316L/NiTi multi-materials with a transition layer produced via SLM. This study is aimed at investigating the influence of a high-entropy alloy (HEA)—CoCrFeNiMn interlayer on the defects' formation, microstructure, phase and chemical compositions, as well as the hardness of the interfacial zone between the HEA and NiTi. The following conclusions are obtained:

(1) The idea of using HEA (CrCoFeNiMn) as an interlayer in the production of 316L/HEA/NiTi multi-material is questionable, since numerous cracks and limited pores occurred in the HEA/NiTi interfacial zone. The interfacial zone has an average size of 100–200 µm.
(2) Microstructure studies indicate that island macrosegregation is formed in the interfacial zone due to the Marangoni effect. The analysis of the phase, chemical composition, and hardness demonstrates that a small amount of FeTi may form in the island macrosegregation. It can be inferred that the presence of a minor amount of FeTi in the interfacial zone results in the formation of the cracks, as this intermetallic compound causes embrittlement.
(3) Further research could involve an in-depth analysis of the phase and chemical composition to confirm the influence of phase formation in the interfacial zone on emerging defects. It would also be pertinent to examine other metals and alloys as interlayers in the 316L/NiTi multi-material.

Author Contributions: Conceptualization, A.R. and A.P.; methodology, A.K.; validation, A.K.; formal analysis, A.K.; investigation, A.R.; resources, A.P.; writing—original draft preparation, A.R.; writing—review and editing, A.R. and A.K.; visualization, A.R.; supervision, A.P.; funding acquisition, A.P. All authors have read and agreed to the published version of the manuscript.

Funding: This research was funded by the Ministry of Science and Higher Education of the Russian Federation (State Assignment for basic research 075-03-2023-004).

Data Availability Statement: The main data have been provided in the paper. Any other raw/processed data required to reproduce the findings of this study are available from the corresponding author upon request.

Conflicts of Interest: The authors declare no conflict of interest.

References

1. Zhang, L.C.; Chen, L.Y.; Zhou, S.; Luo, Z. Powder bed fusion manufacturing of beta-type titanium alloys for biomedical implant applications: A review. *J. Alloys Compd.* **2023**, *936*, 168099.
2. Srivastava, M.; Rathee, S.; Patel, V.; Kumar, A.; Koppad, P.G. A review of various materials for additive manufacturing: Recent trends and processing issues. *J. Mater. Res. Technol.* **2022**, *21*, 2612–2641.
3. Beaman, J.J.; Bourell, D.L.; Seepersad, C.C.; Kovar, D. Additive Manufacturing Review: Early Past to Current Practice. *J. Manuf. Sci. Eng.* **2020**, *142*, 110812.
4. Gunasekaran, J.; Sevvel, P.; Solomon, I.J. Metallic materials fabrication by selective laser melting: A review. *Mater. Today Proc.* **2021**, *37*, 252–256. [CrossRef]
5. Negi, S.; Nambolan, A.A.; Kapil, S.; Joshi, P.S.; Karunakaran, K.P.; Bhargava, P. Review on electron beam based additive manufacturing. *Rapid Prototyp. J.* **2020**, *26*, 485–498. [CrossRef]
6. Sefene, E.M. State-of-the-art of selective laser melting process: A comprehensive review. *J. Manuf. Syst.* **2022**, *63*, 250–274.
7. Wang, D.; Liu, L.; Deng, G.; Deng, C.; Bai, Y.; Yang, Y.; Wu, W.; Chen, J.; Liu, Y.; Wang, Y.; et al. Recent progress on additive manufacturing of multi-material structures with laser powder bed fusion. *Virtual Phys. Prototyp.* **2022**, *17*, 329–365. [CrossRef]
8. Dzogbewu, T.C.; de Beer, D. Powder Bed Fusion of Multimaterials. *J. Manuf. Mater. Process.* **2023**, *7*, 15.
9. Nazir, A.; Gokcekaya, O.; Md Masum Billah, K.; Ertugrul, O.; Jiang, J.; Sun, J.; Hussain, S. Multi-material additive manufacturing: A systematic review of design, properties, applications, challenges, and 3D printing of materials and cellular metamaterials. *Mater. Des.* **2023**, *226*, 111661.
10. Hasanov, S.; Alkunte, S.; Rajeshirke, M.; Gupta, A.; Huseynov, O.; Fidan, I.; Alifui-Segbaya, F.; Rennie, A. Review on Additive Manufacturing of Multi-Material Parts: Progress and Challenges. *J. Manuf. Mater. Process.* **2021**, *6*, 4.
11. Feenstra, D.R.; Banerjee, R.; Fraser, H.L.; Huang, A.; Molotnikov, A.; Birbilis, N. Critical review of the state of the art in multi-material fabrication via directed energy deposition. *Curr. Opin. Solid State Mater. Sci.* **2021**, *25*, 100924.
12. Putra, N.E.; Mirzaali, M.J.; Apachitei, I.; Zhou, J.; Zadpoor, A.A. Multi-material additive manufacturing technologies for Ti-, Mg-, and Fe-based biomaterials for bone substitution. *Acta Biomater.* **2020**, *109*, 1–20. [PubMed]
13. Chen, J.; Yang, Y.; Song, C.; Zhang, M.; Wu, S.; Wang, D. Interfacial microstructure and mechanical properties of 316L /CuSn10 multi-material bimetallic structure fabricated by selective laser melting. *Mater. Sci. Eng. A* **2019**, *752*, 75–85. [CrossRef]
14. Chen, K.; Wang, C.; Hong, Q.; Wen, S.; Zhou, Y.; Yan, C.; Shi, Y. Selective laser melting 316L/CuSn10 multi-materials: Processing optimization, interfacial characterization and mechanical property. *J. Mater. Process. Technol.* **2020**, *283*, 116701.
15. Mei, X.; Wang, X.; Peng, Y.; Gu, H.; Zhong, G.; Yang, S. Interfacial characterization and mechanical properties of 316L stainless steel/inconel 718 manufactured by selective laser melting. *Mater. Sci. Eng. A* **2019**, *758*, 185–191. [CrossRef]
16. Mohd Yusuf, S.; Mazlan, N.; Musa, N.H.; Zhao, X.; Chen, Y.; Yang, S.; Nordin, N.A.; Mazlan, S.A.; Gao, N. Microstructures and Hardening Mechanisms of a 316L Stainless Steel/Inconel 718 Interface Additively Manufactured by Multi-Material Selective Laser Melting. *Metals* **2023**, *13*, 400.
17. Ekoi, E.J.; Degli-Alessandrini, G.; Zeeshan Mughal, M.; Vijayaraghavan, R.K.; Obeidi, M.A.; Groarke, R.; Kraev, I.; Krishnamurthy, S.; Brabazon, D. Investigation of the microstructure and phase evolution across multi-material Ni50.83Ti49.17-AISI 316L alloy interface fabricated using laser powder bed fusion (L-PBF). *Mater. Des.* **2022**, *221*, 110947. [CrossRef]
18. Nie, M.H.; Zhou, Y.X.; Jiang, P.F.; Li, X.R.; Zhu, D.D.; Shan, Z.H.; Chen, Z.K.; Zhang, Z.H. Achieving illustrious friction on a directed energy deposition 316/NiTi heterogeneous alloy with bionic Ni interlayer. *Appl. Surf. Sci.* **2023**, *638*, 158107. [CrossRef]
19. Ng, C.H.; Mok, E.S.H.; Man, H.C. Effect of Ta interlayer on laser welding of NiTi to AISI 316L stainless steel. *J. Mater. Process. Technol.* **2015**, *226*, 69–77. [CrossRef]
20. Shamsolhodaei, A.; Oliveira, J.P.; Schell, N.; Maawad, E.; Panton, B.; Zhou, Y.N. Controlling intermetallic compounds formation during laser welding of NiTi to 316L stainless steel. *Intermetallics* **2020**, *116*, 106656. [CrossRef]
21. Niu, H.; Jiang, H.C.; Zhao, M.J.; Rong, L.J. Effect of interlayer addition on microstructure and mechanical properties of NiTi/stainless steel joint by electron beam welding. *J. Mater. Sci. Technol.* **2021**, *61*, 16–24.
22. Wang, H.; Xie, J.; Chen, Y.; Liu, W.; Zhong, W. Effect of CoCrFeNiMn high entropy alloy interlayer on microstructure and mechanical properties of laser-welded NiTi/304 SS joint. *J. Mater. Res. Technol.* **2022**, *18*, 1028–1037. [CrossRef]
23. Zhang, J.; Yan, Y.; Li, B. Selective Laser Melting (SLM) Additively Manufactured CoCrFeNiMn High-Entropy Alloy: Process Optimization, Microscale Mechanical Mechanism, and High-Cycle Fatigue Behavior. *Materials* **2022**, *15*, 8560. [CrossRef] [PubMed]
24. Zheng, D.; Li, R.; Yuan, T.C.; Xiong, Y.; Song, B.; Wang, J.; Su, Y.D. Microstructure and mechanical property of additively manufactured NiTi alloys: A comparison between selective laser melting and directed energy deposition. *J. Cent. South Univ.* **2021**, *28*, 1028–1042.

25. Deev, A.A.; Kuznetcov, P.A.; Petrov, S.N. Anisotropy of Mechanical Properties and its Correlation with the Structure of the Stainless Steel 316L Produced by the SLM Method. *Phys. Procedia* **2016**, *83*, 789–796. [CrossRef]
26. Soysal, T.; Kou, S.; Tat, D.; Pasang, T. Macrosegregation in dissimilar-metal fusion welding. *Acta Mater.* **2016**, *110*, 149–160. [CrossRef]
27. Wang, J.; Zhu, R.; Liu, Y.; Zhang, L. Understanding melt pool characteristics in laser powder bed fusion: An overview of single- and multi-track melt pools for process optimization. *Adv. Powder Mater.* **2023**, *2*, 100137.
28. Wang, P.; Huang, P.; Ng, F.L.; Sin, W.J.; Lu, S.; Nai, M.L.S.; Dong, Z.L.; Wei, J. Additively manufactured CoCrFeNiMn high-entropy alloy via pre-alloyed powder. *Mater. Des.* **2019**, *168*, 107576.
29. Ge, J.; Yuan, B.; Zhao, L.; Yan, M.; Chen, W.; Zhang, L. Effect of volume energy density on selective laser melting NiTi shape memory alloys: Microstructural evolution, mechanical and functional properties. *J. Mater. Res. Technol.* **2022**, *20*, 2872–2888. [CrossRef]
30. Chen, Y.; Sun, S.; Zhang, T.; Zhou, X.; Li, S. Effects of post-weld heat treatment on the microstructure and mechanical properties of laser-welded NiTi/304SS joint with Ni filler. *Mater. Sci. Eng. A* **2020**, *771*, 138545. [CrossRef]